

Structures and defects of WO_{3-x} nanorods grown by in-situ heating tungsten filament

Huairuo Zhang ^{a,*}, Min Feng ^b, Fei Liu ^b, Libao Liu ^a, Hanyuan Chen ^a,
Hongjun Gao ^b, Jianqi Li ^a

^a Beijing Laboratory of Electron Microscopy, Institute of Physics, CAS, P.O. Box 603-32, Beijing 100080, China

^b Nanoscale Physics and Devices Laboratory, Institute of Physics, CAS, P.O. Box 603-32, Beijing 100080, China

Received 19 February 2004; in final form 22 March 2004

Available online 16 April 2004

Abstract

WO_{3-x} nanorods were grown on the tips of electrochemical etched W filaments by in-situ heating under different growth conditions. This kind of nanorods has the average diameter of 20 nm and the length of 1–2 μm . Transmission-electron microscopy investigations indicate that the sub-stoichiometric WO_3 nanorods, prepared at about 830 °C under the atmosphere of H_2 and Ar mixture, could grow along the either $\langle 001 \rangle$ or $\langle 110 \rangle$ direction with evident stacking faults and textural structure. Nanorods prepared without H_2 atmosphere are found to be respectively $\text{W}_{18}\text{O}_{49}$ grown at around 900 °C and $\text{WO}_{2.9}$ grown at 800 °C.
© 2004 Elsevier B.V. All rights reserved.

1. Introduction

WO_3 and its sub-oxides have been intensively studied for a long time due to their promising physical and chemical properties. For instance, their excellent photo- and electro-chromic properties are commonly used in devices for smart windows [1–4] and information storage [5]. Their ReO_3 -type crystal structures are found to be especially useful in catalytic chemistry [6], intercalation chemistry [4,7], and gasochromic sensors for determination of NO_2 [8], O_3 [9], H_2S [10], NH_3 [11], H_2 [12] and CO [13]. In addition, WO_{3-x} has sheet superconductivity which is closely related to its substructures and defects [14].

Recently, nanomaterials have been widely studied due to their novel properties compared to the corresponding bulk materials. A variety of methods have been developed to prepare tungsten oxides nanoparticles [15], nanotubes [16], nanorods or nanowires [17–19]. In most of these works, the products of tungsten oxides are mixture of WO_3 and its sub-oxides with complex crystallographic defects. It is well-known that certain sig-

nificant properties of the materials are not governed only by the structure of material itself but by faults or defects in the materials. In present work, we prepare tungsten oxide nanorods by heating the electrochemical etched W filaments under different growth conditions. Transmission-electron-microscopy (TEM) observations revealed numerous kinds of planar defects in the nanomaterials. It is also noted that nanorods grown under certain conditions contain well-ordered filament texture structure; this structural feature may be useful in intercalation chemistry for enhancing the diffusion efficiency of intercalation ions.

2. Experimental

Some tungsten tips were prepared by electrochemical etching of tungsten wires, afterward, tungsten tips were mounted on a stainless stage and introduced to an open-ended tube furnace. Three process methods were performed: a batch of tungsten tips were heated at 830 °C for 10 min in a mixture atmosphere of Ar and H_2 with a flow rate of 300, 15 sccm, respectively. Another two batches of tungsten tips were heated at 900 and 800 °C, respectively for 10 min in Ar atmosphere with a same

* Corresponding author. Fax: +86-10-8264-9531/0215.
E-mail address: hrzhang@aphy.iphy.ac.cn (H. Zhang).

flow rate of 300 sccm. FEI XL30 SEM with EDX (energy dispersive X-ray spectroscopy) was used to characterize the as-grown tips. A Hitachi H-9000 TEM and a FEI Tecnai F20 TEM were used to perform the microstructure analysis.

3. Results and discussion

As-grown samples were first investigated by SEM. All the samples have the similar morphological features. Fig. 1a shows a low-magnification top view of one tip with a high concentration of nanorods. These nanorods are highly aligned normal to the metal tungsten surface,

and have the average diameter of 20 nm and the length of 1–2 μm . Fig. 1b displays detailed microstructure features and shapes of the nanorods. This image also directly illustrates the growth process of the sample. The inserted EDX spectrum obtained from the nanorods indicates all peaks can be assigned to the W and O elements (C peak in the EDX data comes from the holder for SEM measurements).

Fig. 2a is a TEM image of one tungsten oxide nanorod grown under 830 $^{\circ}\text{C}$ in the mixture atmosphere of Ar and H_2 . Electron diffraction observations on this kind of nanorods in general give rise to a series of complex weak reflections in the diffraction patterns. Fig. 2b displays a typical electron diffraction pattern with a row of well-defined spots running parallel to the nanorod length axis, and yielding a basic lattice pa-

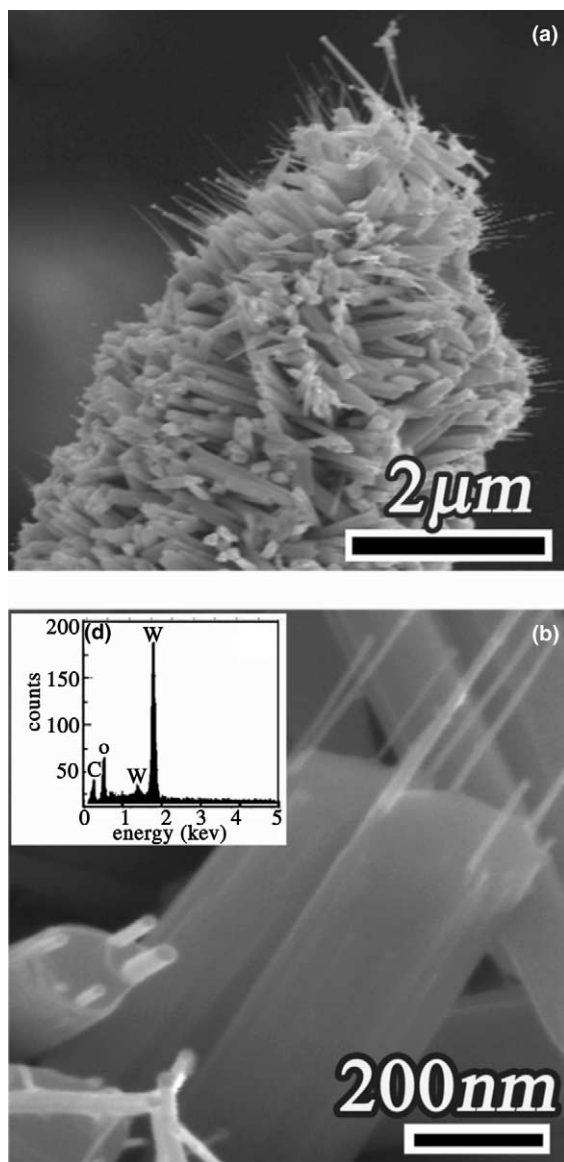


Fig. 1. Representative SEM images of as-grown samples: (a) a low magnification top view of the tip; (b) detailed structure of the nanorods. The inset EDX spectrum was taken from the nanosamples.

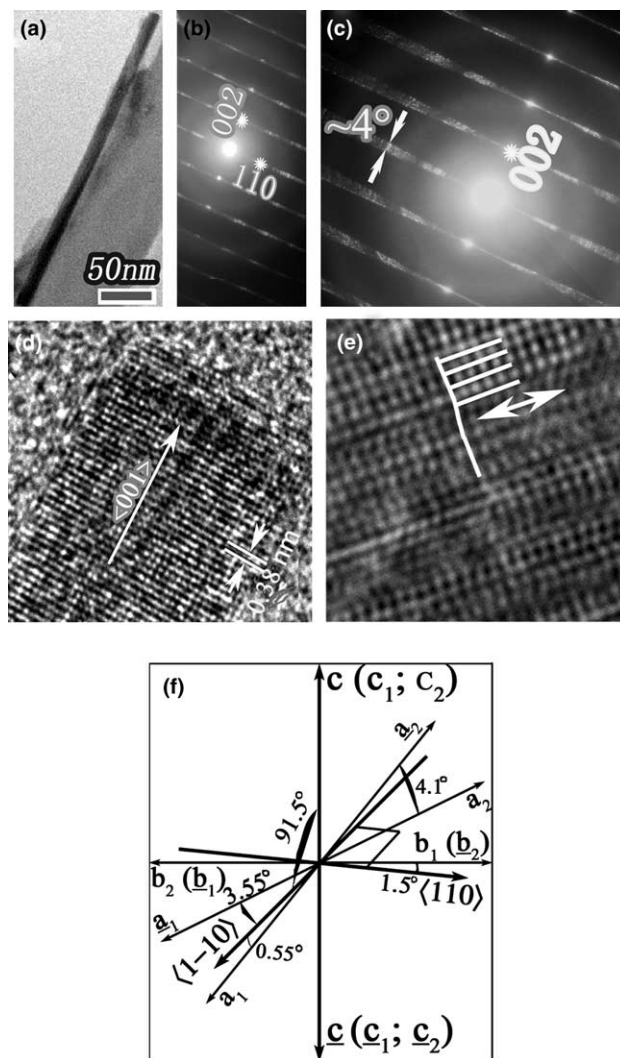


Fig. 2. (a) TEM image of a nanorod grown under 830 $^{\circ}\text{C}$ in the mixture atmosphere of Ar and H_2 . (b) Corresponding EDP of (a). (c) Textured EDP after tilting some degrees subsequent to (b). (d) and (e) HRTEMs corresponding respectively to (b) and (c). (f) Schematic model showing the (001) filament texturing on matrix plane of (001) + (110).

parameter of 0.38 nm. It is notable that other rows of weak diffused spots smeared into streaks running nearly normal to the nanorod length axis. The brighter centers of the diffused spots spaced at distances corresponding to a planar space of about 0.36 nm. As a result of our systematical EDPs measurements of many nanorods, most of the main diffraction spots can be well indexed a monoclinic unit cell with the lattice parameters of $a = 0.5261$ nm, $b = 0.5128$ nm, $c = 0.7650$ nm, and $\beta = 92.05^\circ$, in accordance with the JCPDS card No: 88-0550 for WO_3 , this monoclinic phase has a space group of $P2_1/c$. Moreover, the presence of weak satellite spots and diffuse streaks suggests the existence of certain kind of local modulations and a high density of planar defects along the normal of the nanorod. This structural feature will be discussed in following context based on the HRTEM examinations. In order to well reveal the arrangements of the weak diffraction spots. We tilted the nanorod several degree around the length axis, it is found that the electron diffraction pattern, as displayed in Fig. 2c, shows up a remarkable diffuse sector towards the $\langle 110 \rangle$ direction. The sector in general has an angle of around 4° . This notable feature in electron diffraction patterns commonly observed in many nanorods and can be qualitatively interpreted as the $\langle 001 \rangle$ texture structural behavior existing in this kind of nanorods, which results from crystallites in a nanorod being preferred along the $\langle 001 \rangle$ orientation but with evident declination in certain crystallographic directions. Since the crystal has many local planar defects, we can define it as filament texture. Fig. 2d shows a $[1-10]$ zone-axis HRTEM image of a nanorod directly showing the atomic structure at the top area of the rod, the growth atomic layers can clearly recognized as the (001) crystal planes with a planar distance of about 0.38 nm. Fig. 2e displays a HRTEM image of another nanorod with the similar electron diffraction behavior as shown in Fig. 2c. Some evident superlattice fringes running parallel to length axis can be clear recognized. Structural distortion in correlation with the texture structure is typically indicated by an arrow in the area with evident lattice declination. Fig. 2f is a simple $\langle 001 \rangle$ filament texturing schematic on matrix plane of $\langle 001 \rangle + \langle 110 \rangle$. In this case, the local crystalline lattices textured along whether $\langle 001 \rangle$ or $\langle 00-1 \rangle$ will produce -0.55° or 3.55° off the $\langle 1-10 \rangle$ direction. As a result, the electron diffraction observation reveals a 4° texture sector. Such a case is in good agreement with the diffraction pattern of Fig. 2c. It should be mentioned here that $\langle 110 \rangle$ filament texture was also observed in our samples as shown in Figs. 3c and 4a, and the texturing mechanism discussed above could be used to any other orientation texture.

In order to understand the growth mechanism and microstructure properties of the textured nanorods, we have performed an in-situ heating TEM observation. Fig. 3a is a TEM image of a nanorod for performing the

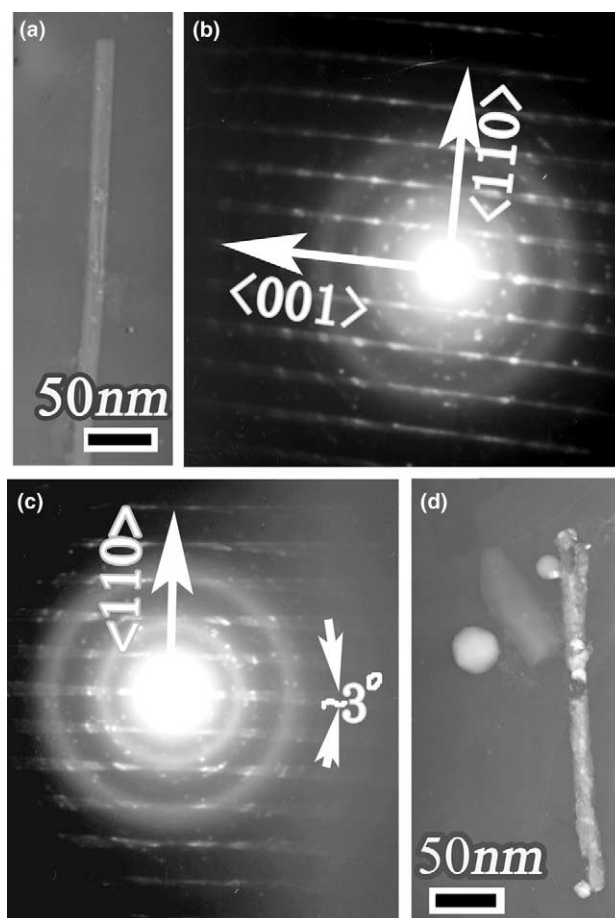


Fig. 3. (a) TEM image and (b) the $\langle 110 \rangle$ texture EDP of a nanorod grown at 830°C for in-situ heating observation. (c) Enhanced texture EDP when heated at 300°C for 40 min. (d) TEM image of a nanorod heated at 650°C , the nanorod was dissolved quickly and nanoparticles were formed nearby.

in-situ heating experiment. Fig. 3b is the corresponding EDP of Fig. 3a showing the observable texture properties along $\langle 001 \rangle$ direction. When temperature rises to 300°C for 40 min, we can clearly see the texture sector with an angle of $\sim 3^\circ$ (characteristic sector angle of $\langle 110 \rangle$ texture). Heated to 530°C , the EDP converted to polycrystalline rings (not shown here), and then the surface of the nanorod started to dissolve slowly. At 650°C , the nanorod dissolved quickly following with the formation of nanoparticles as shown in Fig. 3d. From this heating experiment, it shows that the crystal structure of tungsten oxide nanorod experienced severely transformation at 530°C under non-balance high vacuum atmosphere. It must have experienced deoxygenization and dissociation. Furthermore it suggests that some certain degree of deoxygenization at 300°C results in the enhanced texturing, and the variation of oxygen containing relates closely with texturing. As we know, both H_2 and high-temperature annealing have oxygen reduction effect. In order to seek the origin of such novel texture EDP, we have prepared two more kinds of

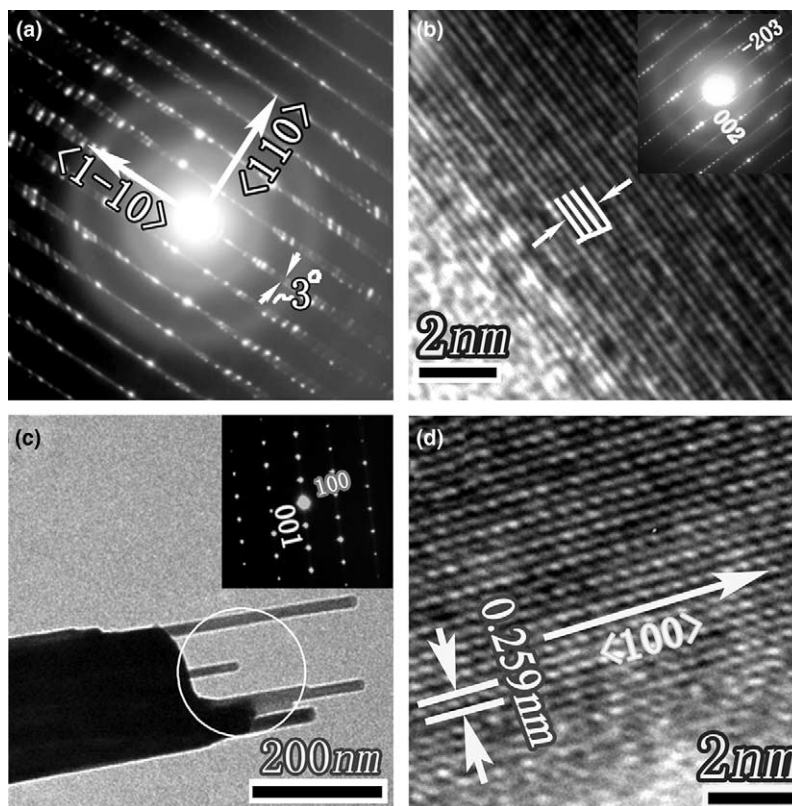


Fig. 4. (a) One representative texture EDP of the nanorods grown at 900 °C without H₂ atmosphere. (b) HRTEM and the EDP of W₁₈O₄₉ taken along the [0 1 0] zone-axis direction. (c) One TEM image of a nanorod grown at 800 °C without H₂ atmosphere, the inset SAEDP taken with some certain degrees off the [0 1 0] zone-axis direction. (d) HRTEM Corresponding to (c) showing the lattice structures of the nanorod.

samples at different temperatures to analogize the experimental results. The first one was grown at higher temperature of 900 °C without H₂ being used. The experimental results indicate a small amount of nanorods with limited texture. Fig. 4a is one of the representative texture EDPs of this sample. Most of as-grown nanorods are identified as stable W₁₈O₄₉ phase, in consistence with the data of JCPDS card No: 84-1516. This phase in general is modulated by crystallographic shear planes or partial vacancy walls [20], our TEM observations clearly reveals the presence of a structural modulation as shown in Fig. 4b. The second sample was grown at lower temperature of around 800 °C and no H₂ was used in the growth process. Nanorods grow on the submicrorod with almost similar shapes as shown in Fig. 4c. The inset selected area electron diffraction pattern (SAEDP) which corresponds to the circle parts containing submicrorod and nanorods suggesting the rods are highly identically orientated. According to the JCPDS card No: 73-2182, electron diffraction patterns obtained from this sample can be indexed by the monoclinic WO_{2.9} (S.G.: *P2/m*, *a* = 1.21 nm, *b* = 0.378 nm, *c* = 2.34 nm, and $\beta = 95^\circ$). No texture phenomenon was observed in this kind of nanorods. Fig. 4d shows a HRTEM image of a nanorod clearly illustrating the substructural lattice with a planar space of about 0.259 nm which is roughly

1/9 of length of *c* axis. It is noted that amorphous layer of about 1nm in thickness is located on the edge of the nanorod which may result from the break of the growth and contamination.

Based on our observations, the experimental results evidently indicate that the H₂ plays an important role for the formation of defects in this kind of nanomaterials, and the texture structure forms irregularly in the growth process: when heated with the presence of H₂, redox competition under oxygen-absence atmosphere results in the oxygen vacancy cluster or sheet in the growth front occasionally, which subsequently leads to W–W bonds formation. Randomly incorporated W–W bond will alter the expected bonding directions and bond lengths, and lowering the structural symmetry, the subsequently followed W–O bonds will have a notable declination at local structure and further shows up as texture structure.

4. Conclusions

Tungsten oxide nanorods were grown on the tip of electrochemical etched tungsten filaments by simply heating under different atmosphere and temperature. When grown under mixture atmosphere of Ar and H₂ at

830 °C, most of the nanorods grow along $\langle 001 \rangle$ or $\langle 110 \rangle$ direction with many defects based on monoclinic WO_3 structure. The complex planar defects and filament texture are commonly observed and purposely result from oxygen vacancy clusters or sheets induced under the competition of redox. When nanorods are grown under atmosphere of Ar at 900 °C, only a small amount of nanorods are textured. Most of the nanorods are found to be typical $\text{W}_{18}\text{O}_{49}$ phase which is stable in high temperature range. Nanorods grown under atmosphere of Ar at 800 °C are found to be crystallized in $\text{WO}_{2.9}$ phase.

Acknowledgements

We would like to thank Prof. Y.Q. Zhou, engineers H.C. Yu and X.A. Yang, for their assistance in experiments.

References

- [1] S.T. Li, M.S. El-Shall, *Nanostruct. Mater.* 12 (1999) 215.
- [2] S.H. Lee, H.M. Cheong, C.E. Tracy, A. Mascarenhas, J.R. Pitts, G. Jorgensen, S.K. Deb, *Appl. Phys. Lett.* 76 (2000) 3908.
- [3] K.S. Ahn, Y.C. Nah, Y.E. Sung, K.Y. Cho, S.S. Shin, J.K. Park, *Appl. Phys. Lett.* 81 (2002) 3930.
- [4] S. Papaefthimiou, G. Leftheriotis, P. Yianoulis, *Electrochim. Acta* 46 (2001) 2145.
- [5] I. Turyan, U.O. Krasovec, B. Orel, T. Saraidorov, R. Reisfeld, D. Mandler, *Adv. Mater.* 12 (2000) 330.
- [6] M. Savanto, J. Raty, T.A. Pakkanen, *Catal. Lett.* 62 (1999) 21.
- [7] R.J.D. Tilley, *Int. J. Refractory Met. Hard Mater.* 13 (1995) 93.
- [8] D.S. Lee, K.H. Nam, D.D. Lee, *Thin Solid Films* 375 (2000) 142.
- [9] W.M. Qu, W. Wlodarski, *Sens. Actuators B* 64 (2000) 42.
- [10] T.L. Royster, D. Chatterjee, G.R. Paz-Pujalt, C.A. Marrese, *Sens. Actuators B* 53 (1998) 155.
- [11] E. Ilobet, G. Molas, P. Molinas, J. Calderer, X. Vilanova, J.E. Sueiras, X. Correig, *J. Electrochem. Soc.* 147 (2000) 776.
- [12] K.H. Lee, Y.K. Fang, W.J. Lee, J.J. Ho, K.H. Chen, K.S. Liao, *Sens. Actuators B* 69 (2000) 96.
- [13] D.S. Venables, M.E. Brown, *Thermochim. Acta* 291 (1997) 131.
- [14] A. Aird, E.K.H. Salje, *J. Phys.: Condens. Matter* 10 (1998) L377.
- [15] S.H. Baeck, T. Jaramillo, G.D. Stucky, E.W. McFarland, *Nano Lett.* 2 (2002) 831.
- [16] Y.B. Li, Y. Bando, D. Golberg, *Adv. Mater.* 15 (2003) 1294.
- [17] G. Gu, B. Zheng, W.Q. Han, S. Roth, J. Liu, *Nano Lett.* 2 (2002) 849.
- [18] Y.B. Li, Y. Bando, D. Golberg, K. Kurashima, *Chem. Phys. Lett.* 367 (2003) 214.
- [19] Y.Q. Zhu, W.B. Hu, W.K. Hsu, M. Terrones, N. Grobert, J.P.H.W. Kroto, D.R.M. Walton, H. Terrones, *Chem. Phys. Lett.* 309 (1999) 327.
- [20] J. Sloan, J.L. Hutchison, R. Tenne, Y. Feldman, T. Tsirlina, M. Homyonfer, *J. Solid State Chem.* 144 (1999) 100.